The Role of the Gamma Function Shape Parameter in Determining Differences between Condensation Rates in Bin and Bulk Microphysics Schemes

Adele L. Igel[1] and Susan C. van den Heever

Department of Atmospheric Science

Colorado State University

Fort Collins, Colorado

[1]Corresponding author:

Department of Land, Air & Water Resources

One Shields Avenue, Davis, CA 95616

aigel@ucdavis.edu

Abstract. The condensation and evaporation rates predicted by bin and bulk microphysics schemes within the same model framework are compared in a novel way using simulations of non-precipitating shallow cumulus clouds. Despite fundamental disparities between the bin and bulk condensation parameterizations, the differences in condensation rates are predominantly explained by accounting for the width of the cloud droplet size distributions simulated by the bin scheme. The bin scheme does not always predict a cloud droplet size distribution that is well represented by a gamma distribution function (which is assumed by bulk schemes); however, this fact does not appear to be important for explaining why the two scheme types predict different condensation and evaporation rates. The width of the cloud droplet size is not well constrained by observations and thus it is difficult to know how to appropriately specify it in bulk microphysics schemes. However, this study shows that enhancing our observations of this width and its behavior in clouds is important for accurately predicting condensation and evaporation rates.

1. Introduction

Bin and bulk microphysics schemes are both popular approaches for parameterizing subgrid-scale cloud processes as evidenced by the large number of schemes that have been developed. Tables 2 and 3 in Khain et al. (2015) summarize the characteristics of dozens of microphysics schemes, and discuss in detail the fundamental principles of these two basic types of schemes. Briefly, in double-moment bulk schemes, the mass mixing ratio and total number mixing ratio for predefined hydrometeor species are predicted, and a function is assumed to describe the shape of the size distribution of each species. In contrast, bin schemes do not assume a size distribution function, but instead, the distribution is broken into discrete size bins, and the mass mixing ratio and/or the number mixing ratio is predicted for each bin.

Bin schemes, particularly those for the liquid-phase, are generally thought to describe cloud processes more realistically and accurately than bulk schemes, and thus they are often used as the benchmark when comparing simulations with different microphysics schemes (e.g. Beheng, 1994; Seifert and Beheng, 2001; Morrison and Grabowski, 2007; Milbrandt and Yau, 2005; Milbrandt and McTaggart-Cowan, 2010; Kumjian et al., 2012). For the ice phase, bin schemes are subject to many of the same issues as bulk schemes, such as the use of predefined ice habits (which may not always appropriately describe real-world ice) and the conversion between ice types (the real atmosphere does not have strict categories for ice), rendering them not necessarily more accurate (Khain et al. 2015). Regardless, bin schemes are much more computationally expensive since many additional variables need to be predicted. As a result, bin schemes are used less frequently than bulk schemes, and are not currently utilized in any operational models. It is of interest then to see how well bulk and the more accurate liquid-phase bin microphysics schemes compare in terms of predicted process rates, and to assess how much predictive value is added by using a bin instead of a bulk microphysics scheme. Furthermore, comparison of process rates in bin and bulk schemes could help to identify ways in which to improve bulk schemes.

One of the primary drawbacks of double-moment bulk schemes that assume probability distribution functions (PDFs) is that many microphysical processes are dependent on the distribution parameters that must be either fixed or diagnosed. In the case of a gamma PDF, which is typically used in bulk schemes, this parameter is the shape parameter. The gamma size distribution (n) is expressed as

$$n(D) = \frac{N}{{D_n}^{\nu}\Gamma(\nu)} D^{\nu-1} e^{-D/D_n} \quad (1)$$

where ν is the shape parameter, N is the number mixing ratio, D is the diameter, and D_n is a scaling diameter (the inverse of D_n is often called the slope parameter). All symbols are defined in Table 1 for reference. Much is still to be learned regarding what the most appropriate value of this parameter is and how it might depend on cloud microphysical properties.

Figure 1 shows previously proposed relationships between the cloud droplet number concentration and the shape parameter (Grabowski, 1998; Rotstayn and Liu, 2003; Morrison and Grabowski, 2007; hereinafter G98, RL03, and MG07, respectively) along with values of the shape parameter reported in the literature and summarized by Miles et al. (2000) for several different cloud types. The figure shows a wide range of possible values of the shape parameter based on observations. The lowest reported value is 0.7 and the highest is 44.6, though this highest point is clearly an outlier. Furthermore, there is no apparent relationship between the shape parameter and the cloud droplet concentration in the data set as a whole, and both increases and decreases of the shape parameter are found with increasing droplet concentration among individual groupings. There is also no clear dependence of the shape parameter on cloud type. Figure 1 additionally shows that two of the proposed functions relating these two quantities are similar (RL03 and MG07), but that the third function (G98) exhibits an opposite trend compared with these first two.

Furthermore, using appropriate values of the shape parameter may be necessary to accurately model cloud characteristics and responses to increased aerosol concentrations. Morrison and Grabowski (2007) found that switching from the MG07 to the G98 N-ν relationships in Figure 1 led to a 25% increase in cloud water path in polluted stratocumulus clouds. This example shows that inappropriately specifying the shape parameter could have implications for the accurate simulation of not only basic cloud and radiation properties but also for the proper understanding of cloud-aerosol interactions. However, it is apparent from Figure 1 that *large uncertainties still exist regarding the behavior of the shape parameter and how it should be represented in models*. The goal of this study is to compare the condensation and evaporation rates predicted by bin and bulk microphysics schemes in cloud-resolving simulations run using the same dynamical and modeling framework and to assess what the biggest sources of discrepancies are. The focus is on condensation and evaporation since these processes occur in all clouds and are fundamental for all hydrometeor species. It will be shown that in spite of other basic differences between the particular bulk and bin microphysics schemes examined here, the lack of a prognosed shape parameter for the cloud droplet size distribution in the bulk scheme is often the primary source of differences between the two schemes. Thus an improved understanding of the shape parameter is necessary from observations and models.

2. Condensation/Evaporation Rate Formulations

The Regional Atmospheric Modeling System (RAMS) is used in this study. It contains a double-moment bulk microphysics scheme (BULK) (Saleeby and Cotton, 2004) and the Hebrew University spectral bin model (BIN) (Khain et al., 2004). The Hebrew University spectral bin model is newly implemented in RAMS. Details about the implementation can be found in Appendix A.

In the BULK microphysics scheme, condensation/evaporation is treated with a bulk approach. Cloud droplet size distributions are assumed to conform to a gamma probability distribution function (PDF) given by Eq. (1). The condensation/evaporation scheme is described in detail in Walko et al. (2000), and the amount of liquid water condensed in a time step is given by their Eq. 6. Here, a slightly rearranged and simplified version of this equation is presented in order to highlight the similarities to the BIN condensation/evaporation equation shown below. Specifically, the BULK condensation/evaporation equation can be written as

$$r_c^{t+\Delta t} = r_c^* + 2\pi\left[N\bar{D}\nu\left(\frac{\Gamma(\nu)}{\Gamma(\nu+3)}\right)^{1/3} f_{\nu,BULK}\right] G_{BULK}(S^{t+\Delta t} - 1)\Delta t \quad (2)$$

The BULK scheme uses this equation for all cloud species, such that the supersaturation is explicitly predicted; a saturation adjustment scheme is not used for cloud water.

In contrast, the equation for the condensation/evaporation rate in the BIN is given by

$$r_c^{t+\Delta t} = r_c^* + 2\pi\left(\sum N_i D_i f_{vi,BIN}\right) G_{BIN} \int_0^{\Delta t}(S-1)dt \quad (3)$$

Semi-analytical equations are used to solve for the time integral of supersaturation that appears at the end of Eq. 3 (Khain and Sednev, 1996). In both equations, r_c is the cloud mass mixing ratio, f_v is the ventilation coefficient, G is a term that accounts for latent heating, vapor diffusion and heat diffusion, S is the saturation ratio, and t is time. The saturation ratio is defined as the ratio of the water vapor partial pressure to the saturated water vapor partial pressure. More details are given in Table 1.

Although both equations have the same basic form, there are two primary differences in how these equations are formulated:

- In the BIN, as is required by the model structure, the condensation rate is calculated for each bin of the distribution, and these rates are then summed over all bins, as opposed to the integration of the gamma distribution that is done in the BULK scheme.
- The time step integration is performed semi-analytically in the BIN with multiple sub-time steps rather than implicitly as in the BULK scheme.

These differences between the bin and bulk schemes will be taken into consideration in this analysis in order to understand why the two schemes produce different condensation rates.

3. Simulations

In order to investigate the difference in condensation rates predicted by the two microphysics schemes, simulations of *non-precipitating* shallow cumulus clouds over land were performed. This cloud type was chosen in order to minimize the indirect impacts of precipitation processes on the analysis. Furthermore, the daytime heating and evolution of the boundary layer results in a wider range of thermodynamic conditions than would occur in simulations of maritime clouds.

The wider range of thermodynamic conditions make the conclusions of this study more robust. The simulations were the same as those described in Igel et al. 2016a-b. They were run with RAMS and employed 50m horizontal grid spacing and 25m vertical grid spacing over a grid that is 12.8 x 12.8 x 3.5 km in size. Such fine grid spacing was used in order to well resolve the cumulus clouds and their microphysical structure. The simulations were run for 9.5 hours using a 1s time step. Clouds appeared after about 4.5 hours. The simplified profiles of potential temperature, horizontal wind speed, and water vapor mixing ratio based on an Atmospheric Radiation Measurement (ARM) Southern Great Plains (SGP) sounding from 6 July 1997 at 1130 UTC (630 LST) presented in Zhu and Albrecht (2003) (see their Fig. 3) were used to initialize the model homogeneously in the horizontal direction. Random temperature and moisture perturbations were applied to the lowest model level at the initial time in order to initiate convection.

Some modifications were made to the model for this study only in order to make the two microphysics schemes more directly comparable. The calculation of the saturation ratio was changed in the BULK scheme to make it the same as the calculation in the BIN. The BIN does not include a parameterization for aerosol dry deposition, so this process was turned off in the BULK scheme. Finally, the regeneration of aerosol following droplet evaporation was deactivated in both microphysics schemes. Aerosol concentrations were initialized homogeneously in the horizontal and vertical directions. Aerosol particles did not interact with radiation.

Five simulations were run with the BULK scheme and three with the BIN scheme. Since the relationships in Figure 1 (G98; RL03; MG07) suggest that the shape parameter may depend on the cloud droplet number concentration, the simulations were run with three different aerosol concentrations, specifically, 100, 400, and 1600 cm^{-3}, in order to obtain a larger range of droplet concentration values. These BULK simulations used a shape parameter value of 4. Two additional BULK simulations were run with an aerosol concentration of 400 cm^{-3} and shape parameter values of 2 and 7. These values were chosen based on previous analysis of the BIN simulations in Igel et al. 2016a. The BIN simulations will be referred to by the microphysics scheme abbreviation and the initial aerosol concentration, e.g. BIN100, and the BULK simulation names will additionally include the value of the cloud droplet shape parameter, e.g. BULK100-NU4.

4. Results

4.1 Instantaneous Condensation Rates

In order to compare directly the condensation rates predicted by the BULK and BIN microphysics schemes, it is necessary to evaluate these rates given the same thermodynamic and cloud microphysical conditions. The BULK condensation equation (Eq. (2)) is approximately linearly proportional to four quantities: S, N, $\bar{D}$, and ν. We say approximately proportional since the presence of the ventilation coefficient (which itself depends on $\bar{D}$ and ν) makes these factors not truly proportional to the condensation rate. In the BIN scheme, among these four variables, the condensation rate is only explicitly proportional to S, and is not explicitly proportional to N, $\bar{D}$, or ν (Eq. (3)) since the BIN scheme does not make assumptions about the functional form of the size distribution. If it is assumed nevertheless that the BIN size distributions *can* be described by some probability distribution function (which does not necessarily have to be a gamma distribution), then we would still expect the BIN scheme condensation rate to scale linearly with N and $\bar{D}$. Therefore, in order to best compare the condensation rates between the two schemes, the condensation and evaporation rates that occur during one time step were binned by the values of S, N, and $\bar{D}$ that existed at the start of the condensation/evaporation process and were averaged in each joint phase space bin. (Note that these phase space bins are not the same is the hydrometeor distribution bins.) That is, all points with the same S, N, and $\bar{D}$ were grouped and the average condensation or evaporation in each group of points was calculated. Saturation ratio bin widths of 0.1 or 1 were used where the cloud was supersaturated or subsaturated, , respectively. For $\bar{D}$, bin widths of 1 μm were used. For N, the bin width depended on the initial aerosol concentration of the simulation: bin widths of 2.5, 10, and 40 mg^{-1} were used for simulations with an initial aerosol concentration of 100, 400, and 1600 mg^{-1}, respectively. The output from the dynamical model only includes the values of S, N, and $\bar{D}$ after condensation and evaporation have occurred. However, since the rates of condensation and droplet nucleation were known from additional model output, and since microphysics was the last physical process to occur during a time step in RAMS, the S, N and $\bar{D}$ that existed before condensation occurred were easily calculated from the model output.

Note that the aerosol activation parameterizations in the BULK and BIN microphysics were not the same, and hence the number of nucleated cloud droplets was not the same. This impacted the number of data points within each joint S, N, and $\bar{D}$ phase space bin. However, we are primarily concerned with the average condensation rate in each phase space bin, and the average value should not be impacted by the number of data points within a phase space bin, provided that the number is sufficiently high (phase space bins with fewer than 50 data points are neglected). Therefore, the differences in the aerosol activation parameterizations, or for that matter, differences in the evolution of the cloud fields, should not influence the differences in the average condensation rates as evaluated in our framework.

The average condensation rate in each S, N, and $\bar{D}$ joint phase space bin was calculated for all simulations. All points where the cloud mixing ratio before condensation was greater than 0.01 g kg^{-1} and the cloud droplet number mixing ratio was greater than 5 mg^{-1} were included in the analysis. In addition, grid points with relative humidity between 99% and 101% *after* condensation or evaporation were excluded. The condensation or evaporation rates at these points were limited by the supersaturation or subsaturation, respectively, and thus the rates were not highly dependent on the droplet characteristics. Since we are interested in understanding how the different representations of droplet distributions impact the condensation and evaporation rates, we do not include these points in our analysis. Finally, as stated above, phase space bins with fewer than 50 data points were discarded. Figure 2 shows an example of the average condensation and evaporation rates in the phase space bins for one simulation. As is seen in Figure 2, there is a smooth transition to higher condensation rates as the saturation ratio increases, and to higher condensation ($S \geq 1$) and evaporation ($S<1$) rates as the droplet diameter or number mixing ratio increases. This is expected based on the condensation equations (Eqs. (2), (3)). All other simulations behave similarly.

In order to compare easily the condensation rates predicted by the two microphysics schemes, we calculate the logarithm of the BULK to BIN condensation and evaporation rate ratios (these values will be referred to as 'ln(ratios)') for five pairs of simulations. Specifically, BULK400-NU2, BULK400-NU4, and BULK400-NU7 are all compared to BIN400, while BULK100-NU2 is compared to BIN100 and BULK1600-NU2 is compared to BIN1600. Histograms of this ratio for all pairs of simulations are shown in Figure 3a-b and Figure 3e-f. This set of ln(ratio) histograms will be referred to as ORIG. The data have been separated into subsaturated (evaporating) and supersaturated (condensing) points. Positive values indicate that the rates in the BULK scheme are larger, and negative values indicate that the rates in the BIN scheme are larger. Values of ± 0.1 (± 0.2) correspond to about a 10% (20%) difference.

First we examine the impacts of increasing aerosol concentrations on evaporation and condensation rates for BULK simulations with the same shape parameter. Figures 3a-b show the histograms of the condensation and evaporation rate ln(ratios) for pairs of simulations with a cloud droplet shape parameter of 4 but with differing initial aerosol concentration. Table 2 additionally lists the standard deviation associated with each histogram. Figure 3a reveals that in general the condensation rate is higher in the BIN scheme simulations as indicated by the more frequent negative ln(ratios), whereas the evaporation rates are more similar between the two scheme as indicated by the most frequent ln(ratios) being equal to 0. For the simulation pair with an initial aerosol concentration of 1600 cm^{-3}, there is a long tail of positive ln(ratio) values. As a result, this pair of simulations has the highest standard deviation of the ln(ratio) values of all simulation pairs (Table 2a).

We now examine the impacts of variations in the shape parameter for a constant aerosol concentration. Figures 3e-f show the histograms of condensation and evaporation rate ln(ratios) for the three BULK400 simulations that have different values of the cloud droplet shape parameter. All three BULK400 simulations are compared to the BIN400 simulation. For both condensation and evaporation, the ln(ratios) increase as the cloud droplet shape parameter used in the BULK400 simulations increases. For the BULK400-NU2 simulation, the condensation and evaporation rates are frequently 20% lower than the BIN400 rates or more, whereas, for the BULK400-NU7 simulation, the condensation rates compared to the BIN400 simulation are most frequently very similar (ln(ratio) near zero). Thus the value of the cloud droplet shape parameter chosen for use in a simulation is clearly important for determining how well a bulk microphysics scheme compares to a bin microphysics scheme in terms of predicted condensation and evaporation rates.

4.2 Impact of the Shape Parameter on Condensation and Evaporation

Fortunately, we know theoretically how the cloud droplet shape parameter will alter condensation and evaporation rates and this dependency can be accounted for in our comparison of the two microphysics schemes. The shape parameter term in Eq. (2) (hereafter f_{NU}), which is equal to $\nu\left(\frac{\Gamma(\nu)}{\Gamma(\nu+3)}\right)^{1/3}$, indicates that when a gamma PDF is assumed, the condensation rate is proportional to the shape parameter v such that a higher shape parameter results in higher condensation rates. The BIN scheme makes no assumptions about the size distribution functionality. However, in order to characterize the predicted BIN cloud droplet size distributions, and to facilitate the comparison of the BIN and BULK condensation rates, we assumed that the predicted BIN size distributions are gamma PDF-like and found the best-fit gamma PDF parameters (see Eq. (1)) for the cloud droplet size distributions at every cloudy grid point in the BIN simulations. (We could just have easily fitted another PDF to the BIN distributions, but chose the gamma PDF since that is what is assumed by most bulk schemes, including the one being used in this study. We examine the appropriateness of this choice in section 4.3.1.) We then evaluated the mean value of f_{NU} using these best-fit shape parameters for each joint bin in the S, N, and $\bar{D}$ phase space.

In order to find the best-fit shape parameters, we defined cloud droplets as belonging to one of the first 15 bins of the BIN liquid array (the remaining 18 bins contain raindrops), which corresponded to a maximum cloud droplet diameter of 50.8 μm. Many methods are available to find such best-fit parameters, but they generally all give similar results (McFarquhar et al., 2014). Here we used the maximum-likelihood estimation method and found best-fits that minimize the error in the total number mixing ratio. Using this method, the size distributions were first normalized by the corresponding total number mixing ratio, leaving only D_n and ν as free parameters of the distribution (Eq. 1).

Note that while we could determine the values of S, N, and $\bar{D}$ that existed before condensation occurred, we could not determine the value of the best-fit shape parameter for this time because the change in mixing ratio of each bin was not output by RAMS. Thus the average shape parameters used in the analysis are those that exist at the end of the time step. Nonetheless, given the short time step used in these simulations, it was not expected that the best-fit shape parameter would change much in one time step in most cases. The exception may be for very broad distributions characterized by low shape parameters. In part due to this concern, cloudy points with best-fit shape parameters less than 1 are not included in the analysis. Overall, the impact of using the post-condensation shape parameters is not expected to have a large impact on the results presented here.

The shape parameter term (f_{NU}) can be evaluated for each joint bin in the S, N, and $\bar{D}$ phase space for all simulations. In the case of each BULK simulations, the value of f_{NU} is the same for every phase space bin since the value of f_{NU} is uniquely determined by the choice of the shape parameter value for each BULK simulation. For the BIN simulations, f_{NU} can be calculated using the best-fit shape parameters. Unlike for the BULK simulations, the value of f_{NU} for the BIN simulations will vary amongst the phase space bins since the best-fit shape parameter is determined from the freely evolving cloud droplet size distributions that are predicted by the BIN microphysics scheme. We can use the values of f_{NU} in our comparison of the condensation and evaporation rates to account for the fact that the best-fit shape parameters in the BIN simulations will often be different from the single prescribed value in the BULK simulations. Specifically, in our analysis (but not in the simulations themselves), we adjusted the mean condensation and evaporation rates (C) *for each phase space bin* from the BULK simulations in the following way:

$$C_{BULK,corrected} = C_{BULK,original} \frac{f_{NU,BIN}}{f_{NU,BULK}} \quad (4)$$

Note again that the value of $f_{NU,BIN}$ will be different for each phase space bin. By making this correction, we found the condensation and evaporation rates that the BULK simulations *would have had* if they had used the same value of the shape parameter that best characterized the cloud droplet size distributions that were predicted by the BIN simulations.

The ln(ratios) of the modified condensation and evaporation rates from the BULK simulations to the rates from the BIN simulations are shown in Figures 3c-d and Figures 3g-h. This set of ln(ratios) will be referred to as CORR. The most frequent value of the CORR ln(ratios) is near zero (indicating that the two schemes predict the same rate) for all simulation pairs and for both condensation and evaporation. The impact of the modification is most notable in Figures 3g-h where the histograms of the CORR ln(ratios) now nearly lie on top of one another whereas in Figures 3e-f they are clearly separated. Thus it appears that our method of accounting for the value of the shape parameter has worked well.

Furthermore, the standard deviation of the condensation rate CORR ln(ratio) histograms is decreased by about half compared to the ORIG ln(ratio) histograms (Table 2a-b). This is not the case for the evaporation rate CORR ln(ratio) histograms where the standard deviation is increased compared to the ORIG ln(ratio) histograms in four out of five simulation pairs. Nonetheless, given that all CORR histograms now have a modal value near 0, whereas this was not the case with the ORIG histograms, the shape parameter appears to be the primary reason why the condensation and evaporation rates in the two schemes do not always agree.

4.3 Other Considerations

While the shape parameter appears to be the primary cause of the differences in condensation and evaporation rates in bin and bulk microphysics schemes, we now investigate whether any of the other factors are also important.

4.3.1 Appropriateness of the Gamma PDF

One potential factor worth considering is that the gamma PDF is not always appropriate for characterizing the cloud droplet size distributions in the BIN simulations. The BIN microphysics scheme is capable of predicting any shape for the cloud droplet size distributions, including size distributions that may be bimodal. To assess how well our fitted gamma PDFs approximated the actual simulated cloud droplet size distributions, we calculated the normalized root mean square error (NRMSE) of the fits. An NRMSE of 1 indicates that the fit was no better than a straight line, and a value of 0 indicates a perfect fit. Figures 4a-b show cumulative histograms of the NRMSE values from the three BIN simulations for both evaporating and condensing cloudy points. Note that these are not cumulative histograms of mean values from joint bins as in Figure 3, but rather they are cumulative histograms of the NRMSE values at all individual cloudy grid points in the BIN simulations. The majority of grid points has NRSME values of 0.6 or lower which indicates that in general the gamma PDF characterizes the simulated cloud droplet size distributions very well.

We repeated the calculations of mean condensation or evaporation rate in each S, N, and $\bar{D}$ joint phase space bin for the BIN simulations, but now we only included those cloudy points with an NRMSE of 0.6 or more (those points with a poor gamma PDF fit). The phase space bins for the BULK simulations were unaltered, but did include the modification described by Eq. (4) which now used values of $f_{NU,BIN}$ based only on the high NRMSE points. The resulting histograms of condensation and evaporation rate ln(ratios) are shown in Figures 5a-b for all simulation pairs. The associated standard deviations are listed in Table 2c. This set of histograms will be referred to as CORR-POOR. For evaporation, the peaks of the CORR-POOR ln(ratios) histograms shift to positive values (Fig. 5a) indicating that the agreement between the BULK and BIN rates is degraded, although the standard deviations of these histograms are similar compared to the CORR histograms (Table 2c compared to Table 2b). The shift in peak ln(ratios) suggests that when the BIN simulations produce cloud droplet size distributions that poorly conform to a gamma PDF, the best-fit shape parameter is less useful for understanding the differences between BULK and BIN evaporation rates.

However, for condensation rates, the results are less clear. Figure 5b shows that many of the high CORR-POOR ln(ratio) histograms are still centered near 0, which indicates that the BIN and modified BULK condensation rates still agree well. Furthermore, the standard deviation of these histograms is similar to those of the CORR histograms (Table 2b-c). Unlike for evaporation, these results for condensation suggest that the fact that the BIN simulations do not predict cloud droplet size distributions that are similar to gamma PDFs is not an important reason for why the BULK and BIN schemes predict different condensation rates. It is unclear why the comparisons of condensation and evaporation rates behave so differently. This uncertainty will be explored next.

4.3.2 Fraction of Cloud Mass Evaporated

One potential reason that evaporation comparison is generally worse than the condensation comparison relates to the fractional change of mass. Specifically, the comparison may be better for situations in which only a small fraction of the total cloud droplet mass is condensed or evaporated within a time step versus a situation in which a large fraction of mass is evaporated. The reason for this is that the BIN microphysics scheme takes an iterative approach to condensation and evaporation in which many small time steps are taken. After each small time step the droplet properties are updated. When the droplet properties are changing rapidly, this approach may be important for accurately predicting the evolution of the total mass and number of cloud droplets. On the other hand, the RAMS bulk scheme takes just one step (which is equal to the full model time step length) and cannot account for rapidly changing droplet properties within the time step. Note that both approaches to the time step during condensation and evaporation could be applied to any bulk microphysics scheme, and hence the differences in condensation and evaporation due to the two approaches are not necessarily specific to differences in bin and bulk schemes. That being said, the behavior associated with each time stepping approach should be similar regardless of the specific scheme that is employing the approach.

Cumulative histograms of the fraction of cloud mass evaporated in one full time step are shown in Figure 4c for the BIN simulations. Higher fractions of mass are evaporated more frequently as the initial aerosol concentration increases. This result is not surprising given that the high numbers of cloud droplets nucleated from the high numbers of aerosol particles will induce, on average, higher evaporation rates (Eq (2) and Eq(3)) that cause a higher fraction of mass to be evaporated in one time step. Similarly, cumulative histograms of the fraction of cloud droplet mass condensed in the time step are shown in Figure 4d. Again, high fractions of cloud mass are condensed more frequently as the initial aerosol concentration increases. Overall, large fractional changes in the cloud mass are more frequent during evaporation than during condensation.

Again, the calculations of mean evaporation rate in each S, N, and $\bar{D}$ joint phase space bin for both the BULK and BIN simulations were repeated but this time with cloudy points separated by low and high mass fraction change. High evaporated mass fraction is defined as 0.25 or higher. Very few cloudy points undergoing condensation have a mass fraction change of 0.25 or higher.

Likewise, very few evaporating cloudy points in BIN100 exceed this threshold. Thus, the following analysis is only performed for the subsaturated, evaporating cloudy points for simulations pairs that include BIN400 or BIN1600.

The evaporation rate ln(ratio) histograms for the two groups (referred to as CORR-LFR and CORR-HFR) are shown in Figures 5c-d and the associated standard deviations are listed in Table 2d-e. It is immediately obvious that the two microphysics schemes behave quite differently for the case of high evaporated fractions. The standard deviation of the CORR-HFR ln(ratio) histograms is up to twice as large as that for ORIG or CORR-LFR (Table 2a,d). Furthermore, most of the CORR-HFR histograms are shifted almost entirely to the right of 0. This result indicates that when the BIN simulations evaporate a high fraction of the cloud mass in one time step, they almost always predict a higher evaporation rate than the BULK simulations when given the same initial cloud properties and relative humidity.

Finally, we found that for grid points at which a high fraction of cloud mass is evaporated, the cloud droplet size distributions predicted by the BIN simulations are more likely to fit poorly to a gamma PDF (not shown). In order to determine which effect was more important, we performed the BULK to BIN evaporation rate comparison twice more: firstly where only BIN simulation points with a high NRMSE of the fitted gamma distributions and a low fraction of cloud mass evaporated were included, and secondly with the opposite conditions where only BIN simulations points with a low NRMSE and a high evaporated fraction were included. The standard deviations of the resultant histograms are listed in Table 2f-g. In the case of high NRMSE and low evaporated fraction, the standard deviations are similar to those for CORR

(Table 2b,f), whereas in the case of low NRMSE and high evaporated fraction the standard deviations are high and are similar to those for CORR-HFR. Thus, it seems that the occurrence of high evaporated fraction is more important for explaining poor agreement between the BULK and BIN microphysics scheme than is a poor fit of a gamma PDF to the cloud droplet size distributions simulated by the BIN scheme.

5. Conclusions

In this study we have compared the cloud condensation rates predicted by a bulk and a bin microphysics scheme in simulations of non-precipitating cumulus clouds run using the same dynamical framework, namely RAMS. The simulations were run with three different background aerosol concentrations in order to consider a large range of microphysical conditions. Two additional simulations with the RAMS bulk microphysics scheme were run with different settings for the cloud droplet shape parameter. When the condensation and evaporation rates were binned by saturation ratio, cloud droplet number mixing ratio, and mean droplet diameter, the BULK rates were on average higher or lower than the BIN rates depending on the value of the shape parameter used in the BULK simulations. Since the theoretical relationship between the shape parameter and condensation/evaporation rates is known, we adjusted the BULK rates to be those that the simulations would have predicted if they had used the same value of the shape parameter as was found by fitting gamma PDFs to the BIN droplet size distribution output. After doing so, we showed that the BULK and BIN rates were in general in much better agreement, although the condensation rates agreed better than the evaporation rates. Additional analysis supported the following conclusions:

1. A gamma probability distribution appears to be a good assumption for the cloud droplet distribution shape, and the exact knowledge of the distribution shape in a bin scheme is often not necessary to minimize errors in the condensation rate in bulk schemes.
2. When a large fraction of the cloud droplet population mass is evaporated within a model time step, the BIN scheme usually predicts lower evaporation rates than the BULK scheme. This appears to be one reason why the evaporation rates comparison is poorer than the condensation rates comparison. It is possible that the multiple sub-time steps taken by the BIN scheme may be important for accurately predicting evaporation rates in either scheme. Such a time-stepping approach could easily be implemented in a BULK scheme. This reason for discrepancy between the two schemes, however, is of secondary importance compared to the shape parameter.

Again, it appears that *the most important factor for agreement in cloud droplet condensation rates between bin and bulk schemes is the shape parameter of the cloud droplet size distribution*. More effort is needed to understand the behavior of the cloud droplet shape parameter in order to improve the representation of cloud droplet size distributions in bulk microphysics schemes.

Although we have only investigated two specific schemes, it is expected that the results can be applied more generally to bulk and bin schemes. Additional work should be conducted using a similar approach in order to compare and evaluate additional microphysics schemes and additional microphysical processes. While it is clear that the effective shape parameter in the bin simulations explains much of the discrepancies in predicted condensation rates between bin and bulk schemes, our understanding of what the most appropriate value of the shape parameter is or how it should vary as a function of basic cloud properties is limited. More work then is therefore also needed on understanding cloud droplet distributions from observations and measurements.

Acknowledgements:

The authors thank Alexander Khain for generously sharing his BIN code in order to make this study possible. This material is based on work supported by the National Science Foundation Graduate Research Fellowship Program under Grant No. DGE-1321845 and the National Aeronautics and Space Administration Grant No. NNX13AQ32G. Additional information can be found in the supporting information or be requested from the corresponding author.

Appendix A

Implementation of the Hebrew University BIN scheme into RAMS

While the present study is only concerned with warm phase processes, the methods to interface the Hebrew University BIN scheme with the RAMS radiation scheme (Harrington, 1997) will be described here for completeness, including those for the ice species. The RAMS radiation scheme uses pre-computed lookup tables for the extinction coefficient, single-scattering albedo, and asymmetry parameter for each hydrometeor species. Three of the hydrometeor species in the BIN correspond directly to species in the RAMS microphysics scheme, namely, aggregates, graupel, and hail. All liquid drops are represented as one species in the BIN, so these liquid bins are classified as either cloud droplets or rain drops using the same size threshold used by the RAMS microphysics scheme to distinguish these two species. Finally, the BIN represents three ice crystal types – plates, columns, and dendrites. Separate RAMS radiation look-up tables already exist for these different ice crystal types, but like for cloud and rain, there are two tables for each crystal type depending on the mean size of the crystals. In RAMS, the small ice crystals are referred to as pristine ice, and the large ice crystals as snow. Again, the same size threshold used to distinguish these two ice categories is used to assign bins from the BIN ice crystal species as either pristine ice or snow. This fortuitous overlap in the ice species has allowed for the seamless integration of the BIN hydrometeor species with the RAMS radiation scheme. For each set of BIN bins that corresponds to a RAMS species, the total number concentration and mean diameter is calculated, a gamma distribution shape parameter of 2 is assumed, and the appropriate set of look-up tables for the corresponding RAMS species is used for all radiative calculations.

References:

Beheng, K. D.: A parameterization of warm cloud microphysical conversion processes, Atmos. Res., 33, 193–206, doi:10.1016/0169-8095(94)90020-5, 1994.

Grabowski, W. W.: Toward Cloud Resolving Modeling of Large-Scale Tropical Circulations: A Simple Cloud Microphysics Parameterization, J. Atmos. Sci., 55(21), 3283–3298, doi:10.1175/1520-0469(1998)055<3283:TCRMOL>2.0.CO;2, 1998.

Harrington, J. Y.: The effects of radiative and microphysical processes on simulation of warm and transition season Arctic stratus, Colorado State University., 1997.

Igel, A. L. and van den Heever, S. C.: The importance of the shape of cloud droplet size distributions in shallow cumulus clouds. Part I: Bin microphysics simulations. Accepted pending revision at J. Atmos. Sci., 2016a.

Igel, A. L. and van den Heever, S. C.: The importance of the shape of cloud droplet size distributions in shallow cumulus clouds. Part II: Bulk microphysics simulations. Accepted pending revision at *J. Atmos. Sci.*, 2016b.

Khain, A., Pokrovsky, A., Pinsky, M., Seifert, A. and Phillips, V.: Simulation of Effects of Atmospheric Aerosols on Deep Turbulent Convective Clouds Using a Spectral Microphysics Mixed-Phase Cumulus Cloud Model. Part I: Model Description and Possible Applications, J. Atmos. Sci., 61(24), 2963–2982, doi:10.1175/JAS-3350.1, 2004.

Khain, A. P. and Sednev, I.: Simulation of precipitation formation in the Eastern Mediterranean coastal zone using a spectral microphysics cloud ensemble model, Atmos. Res., 43(1), 77–110, doi:10.1016/S0169-8095(96)00005-1, 1996.

Khain, A. P., Beheng, K. D., Heymsfield, A., Korolev, A., Krichak, S. O., Levin, Z., Pinsky, M., Phillips, V., Prabhakaran, T., Teller, A., van den Heever, S. C. and Yano, J.-I.: Representation of microphysical processes in cloud-resolving models: Spectral (bin) microphysics versus bulk parameterization, Rev. Geophys., 53(2), 247–322, doi:10.1002/2014RG000468, 2015.

Kumjian, M. R., Ganson, S. M. and Ryzhkov, A. V.: Freezing of Raindrops in Deep Convective Updrafts: A Microphysical and Polarimetric Model, J. Atmos. Sci., 69(12), 3471–3490, doi:10.1175/JAS-D-12-067.1, 2012.

McFarquhar, G. M., Hsieh, T.-L., Freer, M., Mascio, J. and Jewett, B. F.: The Characterization of Ice Hydrometeor Gamma Size Distributions as Volumes in $N_0 - \lambda - \mu$ Phase Space: Implications for Microphysical Process Modeling, J. Atmos. Sci., 72(2), 892–909, doi:10.1175/JAS-D-14-0011.1, 2015.

Milbrandt, J. A. and McTaggart-Cowan, R.: Sedimentation-Induced Errors in Bulk Microphysics Schemes, J. Atmos. Sci., 67(12), 3931–3948, doi:10.1175/2010JAS3541.1, 2010.

Milbrandt, J. A. and Yau, M. K.: A Multimoment Bulk Microphysics Parameterization. Part I: Analysis of the Role of the Spectral Shape Parameter, J. Atmos. Sci., 62(9), 3051–3064, doi:10.1175/JAS3534.1, 2005.

Miles, N. L., Verlinde, J. and Clothiaux, E. E.: Cloud Droplet Size Distributions in Low-Level Stratiform Clouds, J. Atmos. Sci., 57(2), 295–311, doi:10.1175/1520-0469(2000)057<0295:CDSDIL>2.0.CO;2, 2000.

Morrison, H. and Grabowski, W. W.: Comparison of Bulk and Bin Warm-Rain Microphysics Models Using a Kinematic Framework, J. Atmos. Sci., 64(8), 2839–2861, doi:10.1175/JAS3980, 2007.

Rotstayn, L. D. and Liu, Y.: Sensitivity of the First Indirect Aerosol Effect to an Increase of Cloud Droplet Spectral Dispersion with Droplet Number Concentration, J. Clim., 16(21), 3476–3481, doi:10.1175/1520-0442(2003)016<3476:SOTFIA>2.0.CO;2, 2003.

Saleeby, S. M. and Cotton, W. R.: A Large-Droplet Mode and Prognostic Number Concentration of Cloud Droplets in the Colorado State University Regional Atmospheric Modeling System (RAMS). Part I: Module Descriptions and Supercell Test Simulations, J. Appl. Meteorol., 43(1), 182–195, doi:10.1175/1520-0450(2004)043<0182:ALMAPN>2.0.CO;2, 2004.

Saleeby, S. M. and van den Heever, S. C.: Developments in the CSU-RAMS Aerosol Model: Emissions, Nucleation, Regeneration, Deposition, and Radiation, J. Appl. Meteorol. Climatol., 52(12), 2601–2622, doi:10.1175/JAMC-D-12-0312.1, 2013.

Seifert, A. and Beheng, K. D.: A double-moment parameterization for simulating autoconversion, accretion and selfcollection, Atmos. Res., 59-60, 265–281, doi:10.1016/S0169-8095(01)00126-0, 2001.

Walko, R. L., Cotton, W. R., Feingold, G. and Stevens, B.: Efficient computation of vapor and heat diffusion between hydrometeors in a numerical model, Atmos. Res., 53(1-3), 171–183, doi:10.1016/S0169-8095(99)00044-7, 2000.

Zhu, P. and Albrecht, B.: Large eddy simulations of continental shallow cumulus convection,

J. Geophys. Res., 108(D15), 4453, doi:10.1029/2002JD003119, 2003.

Table 1. Definitions of symbols used.

Symbol	Definition
e_s	Saturation water vapor pressure
D	Cloud droplet diameter
$\bar{D}$	Volume mean cloud droplet diameter. $r_c=\pi\rho_w N\bar{D}^3/6$
D_n	Characteristic cloud droplet diameter. $D_n^3=\bar{D}^3\Gamma(v)/\Gamma(v+3)$
$f_{v,BULK}$, $f_{v,BIN}$	Ventilation coefficients for the BULK and BIN schemes, respectively
G_{BULK}, G_{BIN}	Term to account of the impact of latent heat release, vapor diffusion, and heat diffusion on the condensation process. See *Walko et al.* [2000] and *Khain and Sednev* [1996] for the formulations used in the BULK and BIN schemes, respectively. Units are kg m^{-1} s^{-1}.
N	Cloud droplet number mixing ratio
n	Concentration of cloud droplets per unit cloud droplet diameter interval
r_c	Cloud water mass mixing ratio
r_v	Water vapor mass mixing ratio
r_{vs}	Saturated water vapor mixing ratio
S	Saturation ratio
T	Air temperature
t	Time
Γ	Gamma function
v	Gamma distribution shape parameter
( )*	Value of a quantity after advection and all other model processes but before microphysical processes have occurred during a model time step

Table 2. Standard deviation of the ln(ratio) histograms shown in Figures 3 and 5.

	(a) Original, all data (ORIG)	(b) Corrected, all data (CORR)	(c) Corrected, high NRMSE only (CORR-POOR)	(d) Corrected, low fraction mass evaporated (CORR-LFR)	(e) Corrected, high fraction mass evaporated (CORR-HFR)	(f) Corrected, high NRMSE and low fraction mass evaporated	(g) Corrected, low NRMSE and high fraction mass evaporated
Evaporation							
BULK100-NU4/BIN100	0.032	0.025	0.025	-	-	-	-
BULK400-NU4/BIN400	0.044	0.055	0.056	0.041	0.056	0.038	0.054
BULK1600-NU4/BIN1600	0.097	0.120	0.134	0.090	0.160	0.105	0.153
BULK400-NU2/BIN400	0.041	0.054	0.053	0.053	0.046	0.041	0.055
BULK400-NU7/BIN400	0.061	0.072	0.064	0.047	0.087	0.041	0.082
Condensation							
BULK100-NU4/BIN100	0.057	0.033	0.027	-	-	-	-
BULK400-NU4/BIN400	0.056	0.027	0.035	-	-	-	-
BULK1600-NU4/BIN1600	0.057	0.033	0.032	-	-	-	-
BULK400-NU2/BIN400	0.059	0.029	0.032	-	-	-	-
BULK400-NU7/BIN400	0.050	0.026	0.023	-	-	-	-

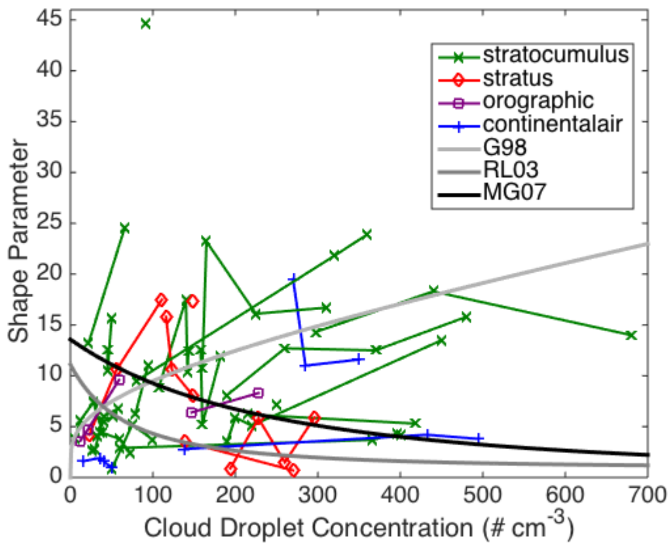

Figure 1. Shape parameter (ν) values as a function of cloud droplet number concentration as reported by Miles et al. (2000) using 16 previous studies. Values, cloud classification, and groupings are based on their Tables 1 and 2. The three solid gray lines show proposed relationships between the cloud droplet concentration and the shape parameter. G98 is from Eq. 9 in Grabowski (1998). RL03 is from Eq. 3 in Rotstayn and Liu (2003) with their α=0.003. MG07 is from Eq. 2 in Morrison and Grabowski (2007). All equations were originally written for relative dispersion, which is equal to $\nu^{-1/2}$, and have been converted to equations for ν for this figure.

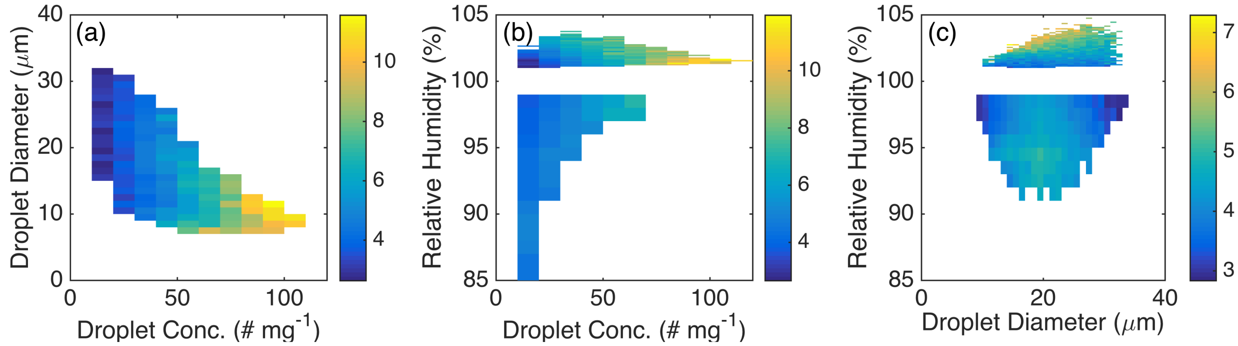

Figure 2. The average condensation and evaporation rates (g kg^{-1} s^{-1}) in joint bins from BIN400. (a) Joint bins where the relative humidity is 101-101.1% (b) Joint bins where the cloud droplet diameter is 18-19 μm. (c) Joint bins where the cloud droplet concentration is 20-21 mg^{-1}. See the text for more information about the joint bins.

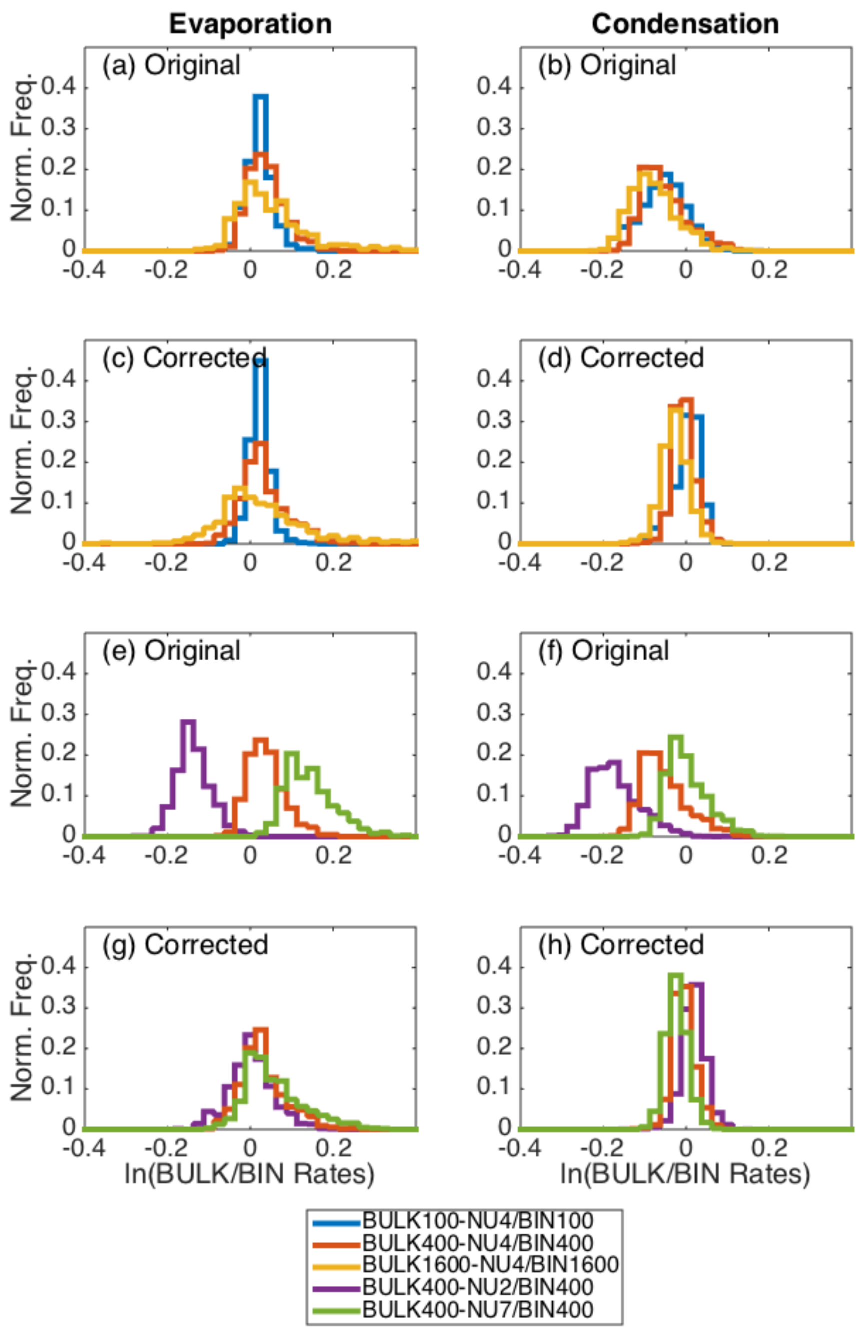

623

624 Figure 3. Normalized histograms showing the logarithm of the ratio of BULK to BIN (a, c, e, g) evaporation and (b, d, f, h) condensation rates. (a-b) and (e-f) show histograms using the original data, and (c-d) and (g-h) show histograms where the correction in Eq. (4) has been applied.

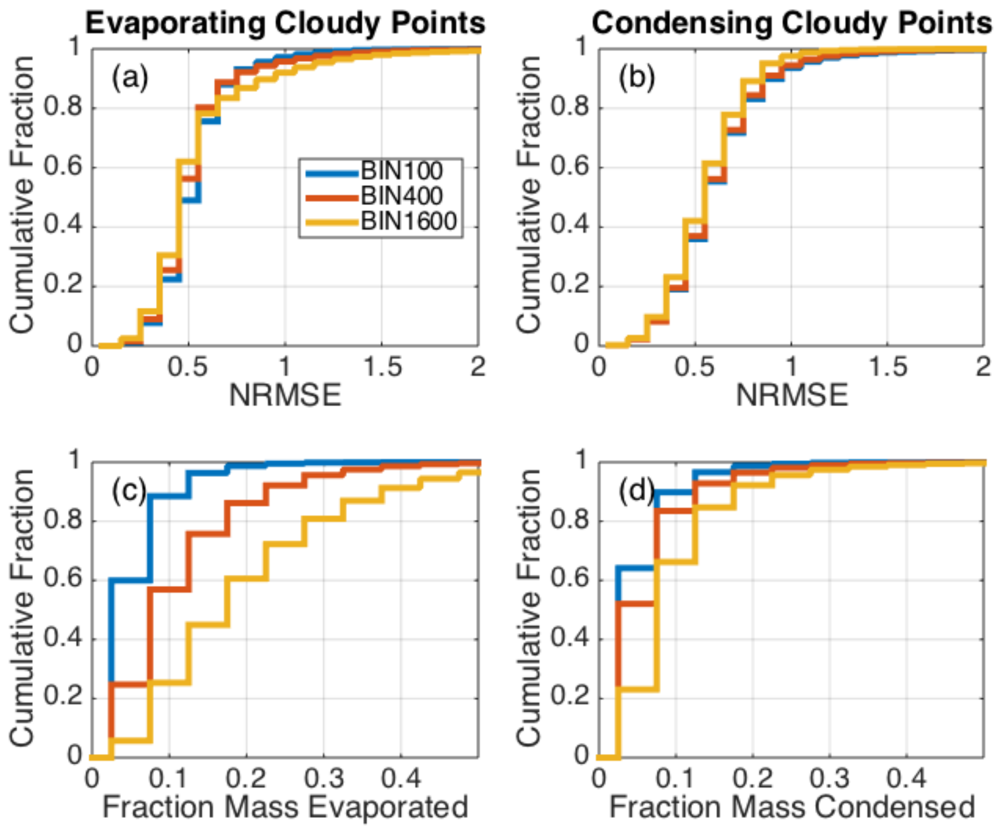

Figure 4. Cumulative histograms of (a-b) the normalized root mean square error (NRMSE) of the fitted gamma PDFs to the simulated cloud droplet size distributions in all three BIN simulations and (c-d) the fraction of cloud mass evaporated or condensed in a time step in all three BIN simulations. (a, c) show evaporating cloudy points and (b, d) show condensing cloudy points.

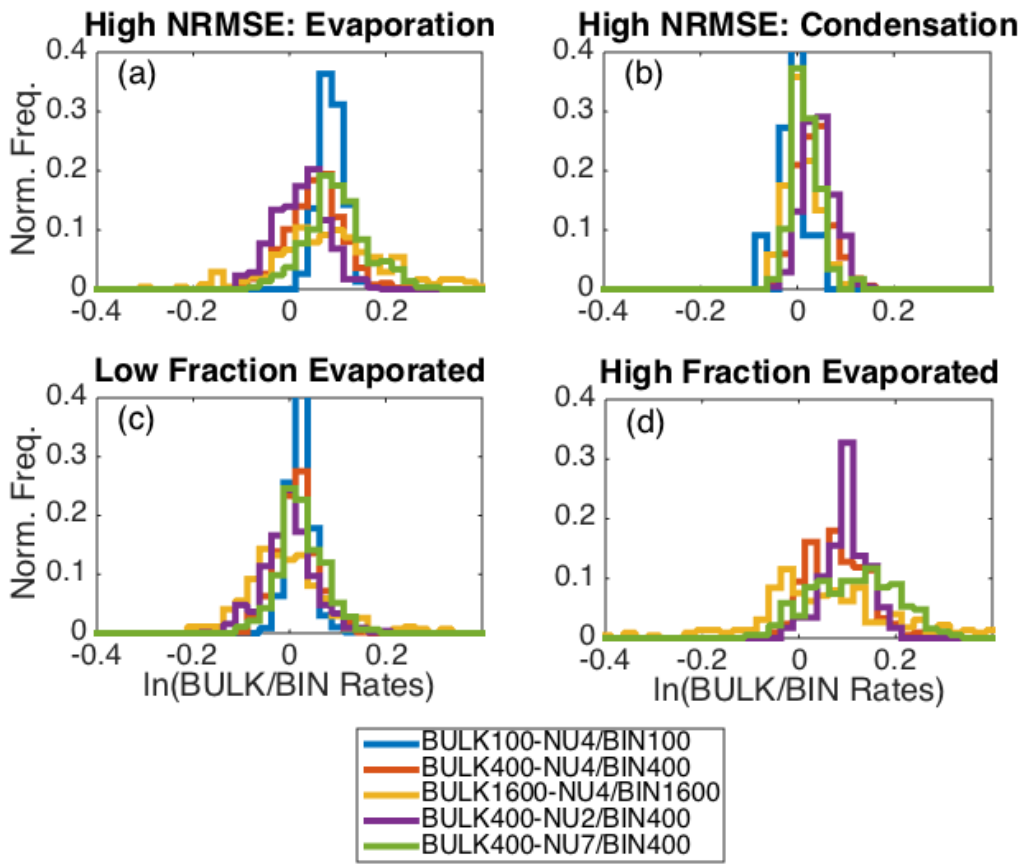

Figure 5. Similar to Figure 3. Histograms of the logarithm of the ratio of BULK to BIN condensation and evaporation rates but with conditional sampling of the data. (a-b) Only BIN simulation data points with an NRMSE greater than 0.6 are included in the analysis. (a) Shows evaporation and (b) shows condensation. (c) Only BIN and BULK simulation data points where the fraction of evaporated mass in one time step is less than 0.25 and (d) where the fraction of evaporated mass is greater than 0.25 are included in the analysis.